EPR, optical absorption and photoluminescence properties of MnO_2 doped $23B_2O_3$-5ZnO-$72Bi_2O_3$ glasses

Shiv Prakash Singh[a], R. P. S. Chakradhar[a], J. L. Rao[b], Basudeb Karmakar[a*]

[a] Glass Technology Laboratory, Glass Division,
Central Glass and Ceramic Research Institute (CSIR), Kolkata-700031, India
[b] Department of Physics, Sri Venkateswara University, Tirupati- 517 502, India.

Abstract

Electron paramagnetic resonance (EPR), Transmission electron microscopy (TEM), optical absorption and photoluminescence (PL) spectroscopic measurements are performed on Mn^{2+} doped high bismuth containing zinc-bismuth-borate glasses. TEM images reveal homogeneously dispersed Bi^o nanopoarticles (NPs) of spherical shape with size about to 5 nm. EPR spectra exhibit predominant signals at $g \approx 2.0$ and $g \approx 4.3$ with a sextet hyperfine structure. The resonance signal at $g \approx 2.0$ is due to Mn^{2+} ions in an environment close to octahedral symmetry; where as the resonance at $g \approx 4.3$ is attributed to the rhombic surroundings of the Mn^{2+} ions. The hyperfine splitting constant (A) indicates that Mn^{2+} ions in these glasses are moderately covalent in nature. The zero-field splitting parameter D has been calculated from the allowed hyperfine lines. The optical absorption spectrum exhibits a single broad band centered around 518 nm (19305 cm^{-1}) was assigned to the $^6A_{lg}(S) \rightarrow {}^4T_{lg}(G)$ transition of Mn^{2+} ions. The visible and near infrared (NIR) luminescence bands at 548, 652 nm, and 804 nm has been observed when excited at 400 and 530 nm respectively. These luminescence centers are supposed to be caused by the lower valence state of bismuth, such as Bi^{2+} and Bi^{+} ions, generated during melting process.

Keywords: Glasses; Mn^{2+} ions; EPR; TEM; Optical absorption; Photoluminescence

* Corresponding author. Tel.: +91 33 2473 3496; fax: +91 33 2473 0957.

E-mail address: basudebk@cgcri.res.in

1. Introduction

Now-a-days, heavy metal oxide (HMO) based glasses such as bismuth oxide based glasses have attracted the scientific community due to its important applications of thermal and mechanical sensors, reflecting windows, glass ceramics etc. [1-4]. Bi_2O_3 possess high refractive index, and exhibit high optical basicity, large polarizibilty and large optical susceptibility values [5-7] which make them ideal candidates for applications as infrared transmission components, ultra fast optical switches, and photonic devices. Moreover, the HMO such as lead or bismuth oxide containing glasses shows extremely high radioactive resistance because of their high density and atomic number. Bismuth oxide alone cannot be considered as network former due to small field strength ($z/a^2 = 0.53$, where z = formal valency and a = internuclear distance) of Bi^{3+} ion [8]. However, in combination with other glass formers, the glass formation is possible in a relatively larger composition range [9].

As a part of our programme on bismuth borate glasses, the authors are interested to prepare high bismuth containing zinc-bismuth-borate glasses. Zinc oxide based glasses/ceramics have special applications in the area of varistors, dielectric layers and transparent dielectric and barrier ribs in plasma display panels [10, 11]. We have undertaken the present work to analyze the influence of MnO_2 on the structure and optical properties of the zinc bismuth borate glasses. Among all the transition metal ions, manganese (Mn) ion is particularly interesting because it exists in different valence states in different glass matrices [12-15]. With the composition of the glass, the local environment of the transition metal (TM) ion incorporated into the glass network can be

changed, leading to local ligand field in homogeneities. The study of such glasses with various spectroscopic techniques will give valuable information on these systems.

2. Experimental

The starting chemicals used in the present study were bismuth trioxide, Bi_2O_3 (Loba Chemie), boric acid, H_3BO_3 (Loba Chemie), zinc oxide, ZnO (Loba Chemie) and manganese dioxide, MnO_2 (Loba Chemie) as raw materials to prepare glasses. The glass of 25 g batch with composition wt % $23B_2O_3$-5ZnO-$72Bi_2O_3$-xMnO_2 (where x = 0, 0.0012, 0.003 and 0.0058 atom % in excess) were melted in a 60 ml platinum crucible at 1150^oC in air for 30 min. with intermittent stirring for 0.5 min. in the electrical furnace. The molten glass was casted onto a carbon plate and annealed at 420^oC for 2h to release the internal stresses. The samples are identified as (a), (b), (c), and (d) with the value of x = 0, 0.0012, 0.003 and 0.0058 atom % respectively. The samples of about 2 ± 0.01 mm thickness were prepared by cutting, grinding and polishing for optical measurements.

The Transmission Electron Microscopy (TEM) and Selected Area Electron Diffraction (SAED) images were taken using a FEI instrument (Tehnai-30, ST G^2) operating at an accelerating voltage of 300 kV. The EPR spectra were recorded on a EPR spectrometer (JEOL-FE-1X) operating at the X-band frequency (≈ 9.200 GHz) with a fields modulation frequency of 100 kHz. The magnetic field was scanned from 0 to 500 mT and the microwave power used was 5 mW. A powdered glass sample of 100 mg was taken in a quartz tube for EPR measurements. The UV-Vis absorption spectra in the range of 400-1100 nm were recorded using a double beam UV-visible spectrophotometer (Lambda 20, Perkin-Elmer) at an error of $\pm$0.1 nm. The fluorescence spectra were

measured at an error of $\pm$0.2 nm with a fluorescence spectrophotometer (Fluorolog 2, Spex) using a 150 W Xe lamp as the excitation source and a photomultiplier tube (PMT) as detector. The excitation slit (1.25 mm) and emission slit (0.5 mm) were kept uniform for luminescence measurement of all the samples.

3. Results and discussion

3.1 Transmission Electron Microscopy studies

The TEM images of samples (a) and (d) are shown in the Fig 1. It clearly reveals homogeneously dispersed Bi^o nanoparticles (NPs) of spherical shape with size about to 5 nm. The particle size of the Bi^o NPs in base glass (sample a) and MnO_2 doped glass (sample d) show similar size (about 5 nm). But the sample (d) showing less dense than the sample (a) because it restricted the further formation of bismuth NPs effectively due to MnO_2 has higher reduction potential Mn^{4+}/Mn^{2+} (E^o = 1.224 V) than that of Bi^{3+}/Bi^o (E^o = 0.308 V) [16]. Therefore, MnO_2 doped glass has not shown densely embedded bismuth NPs. The SAED images of the samples (a) and (d) in Fig. 1 have not shown any distinct spots. This indicates that the particle sizes are very small.

3.2 Electron Paramagnetic Resonance studies

Fig. 2 shows the EPR spectra of $23B_2O_3$-5ZnO-$72Bi_2O_3$-xMnO_2 (where, x = 0.0012, 0.003 and 0.0058 atom %, in excess) glass samples at room temperature. All the samples exhibit two resonance signals at $g \approx 2.0$ and $g \approx 4.3$. Interestingly, the resonance signals observed at $g \approx 2.0$ and $g \approx 4.3$ show predominant six line hyperfine structure (hfs) due to interaction of electron spin (S = 5/2) of Mn^{2+} ions with nuclear spin I = 5/2.

The EPR spectrum of powder sample was analyzed in order to obtain spin-Hamiltonian parameters. The following spin-Hamiltonian has been taken into account [17].

$$H = ßB.g.S + D\,[S_Z^{\,2} - \{S\,(S+1)\,/\,3\}] + I.A.S \qquad (1)$$

where the first term represents the electronic Zeeman term, second term characterize the zero-field splitting of the sextet ground state and the third term represents the hyperfine interaction.

In oxide glasses, the hyperfine structure at $g \approx 4.3$ resonance was detected only in a few cases [18-20]. In binary borate glasses, it has been reported that only $g \approx 2.0$ resonance was well resolved whereas the resonance at $g \approx 4.3$ is less intense and is not resolved [21-24]. In these glasses, B_2O_3 is glass former which allows the Mn^{2+} to enter in the matrix mostly in high symmetry sites there by showing only $g \approx 2.0$ resonance.

In case of d^5 metal ions, it is known that the axial distortion of octahedral symmetry gives rise to three Kramers doublets $|\pm 5/2>$, $|\pm 3/2>$ and $|\pm 1/2>$ [17]. An application of Zeeman field will split the spin degeneracy of the Kramers doublets. As the crystal field splitting is normally much greater than the Zeeman field, the resonances observed are due to transitions within the Kramers doublets split by the Zeeman field. The resonance at $g = 4.3$ are attributed to the rhombic surroundings of the Mn^{2+} ions and arise from transitions between the energy levels of the middle Kramers doublet $|\pm 3/2>$. The resonance at $g \approx 2.0$ is due to Mn^{2+} ions in an environment close to an octahedral symmetry and is known to arise from the transition between the energy levels of the lower doublet $|\pm 1/2>$.

In the present study, we have prepared zinc bismuth borate glasses which impose much more complicated structure compared to binary borate glasses thereby the Mn^{2+} ions structures its vicinity in a constrained space subjected to closer impact with the neighbors. The manganese ions entering in the glass matrix revealed isolated ions ordering their vicinity in regular configuration in distorted sites subjected to high crystal field effects, giving $g \approx 4.3$ resonance signals. These sites are ordered well enough to allow the hyperfine structure good resolution. In addition, the less ordered configurations of Mn^{2+} ion vicinity also revealed the sites with $g \approx 2.0$ resonance signals. The high degree of ordering in the Mn^{2+} ions neighborhood is attested by the good resolution of the hyperfine structure observed at $g \approx 4.3$ resonance signals.

The ability to observe the ^{55}Mn hyperfine structure has two tangible benefits. (1) It generally allows unambiguous assignments of positions of complex resonance lines to manganese; (2) the magnitude of hyperfine splitting constant provides a measure of bonding between Mn^{2+} ion and its surrounding ligands [25, 26]. Their relative intensity varies with the glass structure and composition.

The values of hyperfine splitting constant, A, were determined from the average value of hyperfine splitting of successive allowed hyperfine lines of the central sextet observed for $g \approx 4.3$ and $g \approx 2.0$ resonances. It is apparent from different average values of A measured from peak to peak (A_{pp}) and trough to trough (A_{tt}), that the individual lines are strain broadened, leading to an asymmetry in the absorption spectrum [27]. The first derivative spectrum as a consequence, shows larger values of *A*, when measured trough to trough, rather than peak to peak. An overall average was calculated for both $g \approx 2.0$ and $g \approx 4.3$ resonances from

$$A_{avg} = [(\Delta_{Opp} + \Delta_{Ott}) / 5 + (\Delta_{Mpp} + \Delta_{Mtt}) / 3 + (\Delta_{Ipp} + \Delta_{Itt})] / 6 \qquad (2)$$

where Δ_{Opp} and Δ_{Ott} represent the differences between the first and sixth peak positions, measured peak to peak and trough to trough respectively. Δ_{Mpp} and Δ_{Mtt} represents difference in positions between second and fifth peaks and Δ_{Ipp} and Δ_{Itt} between second and third peaks respectively. It is interesting to note that, in all the samples, $\Delta_{Opp} /5 \approx \Delta_{Mpp} /3 \approx \Delta_{Ipp}$ and $\Delta_{Ott} / 5 \approx \Delta_{Mtt} / 3 \approx \Delta_{Itt}$.

The strength of the hyperfine splitting (*A*) depends on the matrix into which the ion is dissolved and is mainly determined by the electronegativity of the neighbours. This means a qualitative measure of the covalency of the bonding in the matrix which can be determined from the value of *A*; the smaller the splitting, the more covalent the bonding of the anion. The hyperfine splitting (*A*) evaluated for the resonance signals at $g \approx 4.3$ and $g \approx 2.0$ with composition is given in parenthesis. For $g \approx 4.3$ resonance, the hyperfine splitting (A) for 0.0012 atom % of Mn (85 *G*), 0.003 atom % of Mn (83 *G*), 0.0058 atom % of Mn (81 *G*); for the resonance signal at $g \approx 2.0$, the hyperfine splitting (*A*) for 0.0012 atom % of Mn (84 *G*), 0.003 atom % of Mn (90 *G*), 0.0058 atom % of Mn (91 *G*). It is interesting to find that, the hyperfine splitting constant (*A*) for the resonance signal at $g \approx 4.3$ decreases from 85 to 81 gauss with increase of Mn content whereas for $g \approx 2.0$ resonance signal it has increased from 84 *G* to 91 *G* which in turn reflect that there is an increase of covalence character with Mn doping around $g = 4.3$ and decrease of covalence character around $g = 2.0$. These changes are due to ligand field fluctuations around Mn ions, which are strongly dependent on the composition. The magnitude of the hyperfine splitting constant (*A*) in the present study indicates that there exists a moderately covalent bonding between Mn^{2+} ions and the surrounding ligands.

3.3 Calculation of the zero-field splitting parameter (D) from EPR spectra

The intensity of hyperfine lines can be used to calculate the zero-field splitting parameter (*D*) from the ratio of allowed hyperfine lines (corresponding to the selection rule $\Delta m_I = 0$) using the formula [28].

$$I_m \propto 2 - \frac{A^2\left(35-4m^2\right)}{2\left(g\beta H\right)^2} - \frac{5.334D^2}{\left(g\beta H\right)^2} - \frac{35.14D^2\left(35-4m^2\right)}{\left(g\beta H\right)^2} + \frac{208D^4\left(35-4m^2\right)^2}{\left(g\beta H\right)^4} \qquad (3)$$

where m is the nuclear spin magnetic quantum number, I_m is the intensity of the m^{th} allowed hyperfine (HF) line, *A* is the HF splitting constant, *D* is the zero-field splitting parameter and the rest of the symbols have their usual meaning.

The authors have calculated *D* values for $23B_2O_3$-5ZnO-$72Bi_2O_3$-*x*MnO_2 (where, *x* = 0.0012, 0.003 and 0.0058 atom %, in excess) glass samples at room temperature from the ratio of 5/2 ↔ 5/2 hyperfine line intensity to that of the 3/2 ↔ 3/2 hyperfine line for the resonance signal at $g \approx 2.0$. It is observed that the D values are found to decrease from 270 G, 246 G and 234 G when the concentration of manganese increases from (0.0012, 0.003 and 0.0058 atom % respectively. The *D* values obtained from the ratio of the allowed hyperfine line intensities is of the same order for as the *D* values of Mn^{2+} ions reported in literature [28,29].

3.4. UV-VIS-NIR Absorption Studies

The color of the as prepared glass changes gradually as MnO_2 concentration increases in the glass. The as prepared base glass which is deep black in color, after addition of 0.0012, 0.003 and 0.0058 atom % of MnO_2 the glass color changes to brown, light brown and brick red respectively. The measured UV–Vis optical spectra of the undoped and 0.0012, 0.003 and 0.0058 atom % of MnO_2 doped in $23B_2O_3$-5ZnO-

$72Bi_2O_3$ (wt. %) glasses reveal spectral changes. The undoped $23B_2O_3$-5ZnO-$72Bi_2O_3$ (wt. %) glass system and low content (0.0012 atom %) of MnO_2 doped glass has not shown any absorption peaks from 400–1100 nm (Fig. 3). But a weak absorption band at 518 nm begins to appear when MnO_2 concentration is ≥ 0.003 atom %. The glass doped with 0.0058 atom % of MnO_2 reveals (Fig. 3) distinct visible broad absorption at about 518 nm (19305 cm^{-1}). This band is assigned to the $^6A_{1g}(S) \rightarrow {}^4T_{1g}(G)$ transition of Mn^{2+} ions [30]. The Mn^{2+} ion has a ground state of $^6A_{1g}$ in octahedral symmetry, which is lowest according to Hund's rule. Since all the excited states of the Mn^{2+} ion (d^5 configuration) will be either quartets or doublets, the optical absorption spectra of Mn^{2+} ions will have only spin forbidden transitions. On progressively increase in concentration of MnO_2, the broad absorption bands gradually form and prominently distinct at 0.0058 atom % concentration. From EPR and optical absorption studies it is evident that the manganese ions in these glasses are in 2+ valence states. Mn^{2+} ions are generated from MnO_2 through a redox reaction with Bi^{2+} and Bi^{+} originated from Bi_2O_3 at the melting temperature of glass (as discussed in later section) as follows:

$$Mn^{4+} + 2Bi^{2+} \rightarrow Mn^{2+} + 2Bi^{3+} \quad (4)$$

$$Mn^{4+} + Bi^{+} \rightarrow Mn^{2+} + Bi^{3+} \quad (5)$$

Since the glasses (b), (c) and (d) containing low concentration of MnO_2 do not import blackening due to Bi^o formation (as in earlier discussion) and exhibit comparatively more transparency than that of base glass (0 atom % of MnO_2). This fact is also evidenced from transmission electron microscopy (TEM) shown in Fig. 1. Therefore, addition of

MnO_2 is found effective for removing blackening or browning color of high bismuth glasses.

3.5 Photoluminescence studies

During the melting process the Bi^{3+} ion of Bi_2O_3 molecule disproportionate to its lower valence state by auto thermal reduction as follow [31, 32]

$$Bi^{3+} \leftrightarrow Bi^{2+} \leftrightarrow Bi^{+} \leftrightarrow Bi^{o} \qquad (6)$$

Therefore, in the bismuth glass, various valence states of Bi ions may be present. The photoluminescence measurement was carried out for base glass (sample a) and MnO_2 doped glasses (samples b, c and d). Three emission peaks were observed at 548, 650 nm, and at 804 nm when excited at 400 and 530 nm respectively. Zhou et al. [33] explained the various energy levels of Bi ions such as Bi^{3+}, Bi^{2+} and Bi^{+}. In the present study, the observed emission bands are attributed to Bi^{2+} and Bi^{+} ions by considering the energy matching condition with the Zhou et al. [33]. In Bi^{2+} ion a single electron is available in the outer 6p orbital and it is split by spin orbit coupling interaction into $^2P_{1/2}$ and $^2P_{3/2}$ in order of increasing energy. According to the energy level diagram proposed by Zhou et al. [33], the energy level at $^2P_{3/2}$ is further split into two crystal field terms; i.e., $^2P_{3/2}$ (1) and $^2P_{3/2}$ (2). The excitation at 400 nm is attributed to $^2P_{1/2} \rightarrow {}^2P_{3/2}$ (2) transition. The emission bands at 548 nm can be ascribed to $^2P_{3/2}$ (1) $\rightarrow {}^2P_{1/2}$ transition. The red emission band at 650 nm can also be attributed to Bi^{2+} ion as Hamstra et al. [34] have found Bi^{2+} emission band at 625 nm in alkaline-earth-metal sulphates.

The ground state configuration of Bi^+ ($6s^26p^2$) is split by spin-orbit coupling interaction into the ground state $^3P_0$ and the excited states $^1S_0$, $^1D_2$ and $^3P_2$. When the sample is excited at 530 nm, which arises due to $^3P_0 \rightarrow {}^1S_0$ transition, an emission band observed in the infrared region at 804 nm. According to energy level diagram of Zhou et al. [33] and Meng et al. [35] this emission band is attributed to $^3P_2 \rightarrow {}^3P_0$ transition based on the energy matching conditions.

The intensity of the peak at 650 nm and 548 nm in Fig. 4 decreases with increase in MnO_2 concentration from 0.0012 to 0.003 atom %. But, intensity increases in 0.0058 atom % of MnO_2 doped glass of sample (d). The intensity of the both the peaks (548 and 650 nm) is almost same for samples (a), (b) and (c) but in case of the sample (d), the emission peak at 548 nm shows less intensity than that of 650 nm peak. This happened because the sample (d) shows an absorption peak at 518 nm for which the intensity might be decreased due to the absorption of energy by the active ion center. The intensity of the peak at 804 nm in Fig. 5 increases with the increase in concentration of MnO_2 up to 0.003 atom %. But it decreases with the maximum concentration (0.0058 atom % of MnO_2). This may be due to strong absorption band appeared at 518 nm of Mn^{2+} ions by the sample (d), indicating that the excitation energy losses due to absorption of the energy by the Mn^{2+} ion.

4. Conclusions

The TEM images of the investigated samples reveal the formation of Bi nanometals in the glass. The EPR spectra exhibits sextet hyperfine structure (hfs) centered at $g \approx 2.0$ and $g \approx 4.3$. The resonance signal at $g \approx 2.0$ is due to Mn^{2+} ions in an environment close to octahedral symmetry, whereas the resonances at $g \approx 4.3$ are

attributed to the rhombic surroundings of the Mn^{2+} ions. The UV-Vis absorption spectra show a characteristic absorption band of Mn^{2+} at 518 nm which is due to $^6A_{1g}(S) \rightarrow {}^4T_{1g}(G)$ transition. When the glass samples were excited at 400 nm, the photoluminescence centered at 548 and 650 nm was observed which may be due to Bi^{2+} ion. The intensity of the emission peaks is gradually decreases with the increase of MnO_2 concentration up to 0.003 atom % but the intensity increases at highest concentration (0.0058 atom %). The luminescence centered at 804 nm was observed when excited at 530 nm, which may be attributed to Bi^{+} ion. The intensity of the Bi^{+} emission band increases up to 0.003 atom % concentration of MnO_2 and with further addition of MnO_2 (0.0058 atom %) in the glass matrix its intensity decreases. This indicates that the addition of MnO_2 affects the luminescence properties due to redox reaction with the various valence states of bismuth ions.

Acknowledgements

The authors gratefully acknowledge the financial support of NMITLI, CSIR, New Delhi. They gratefully thank Dr. H. S. Maiti, Director of the institute for his keen interest and kind permission to publish this paper. The technical support provided for TEM by the Electron Microscope Division of this Institute is also thankfully acknowledged.

References

[1] C. Stehle, C Vira, D. Vira, D. Hogan, S. Feller, M. Affatigato, Phys. Chem. Glasses 39 (1998) 83.

[2] R. Luciana, P. Kassab, H. Sonia Tatumi, C.M.S. Mendes, Lilia C. Courrol, Niklaus U. Wetter, Opt. Express 6 (2000) 104.

[3] Y. Cheng, H. Xiao, W. Guo, Mater. Sci. Eng. A 480 (2008) 56.

[4] A.A. Ali, M.H. Shaaban, Physica B 403 (2008) 2461.

[5] V. Dimitrov, T. Komatsu, J. Non-Cryst. Solids 249 (1999) 160.

[6] S. Sindhu, S. Sanghi, A. Agarwal, V.P. Seth, N. Kishore, Mater. Chem. Phys. 90 (2005) 83.

[7] X. Zhao, X. Wang, H. Lin, Z. Wang, Phisica B, 390 (2007) 293.

[8] M. B. Volf, *Chemical Approach to Glass*, Elsevier, Amsterdam,1984, p.118.

[9] K. Gerth, C. Russel, J. Non-Cryst. Solids 221 (1997) 10.

[10] A. Lagrange, in B. C. H. Steele (Ed.), Electronic Ceramics : Present and Future of Zinc Oxide Varistors, Elsevier, Cambridge, 1991. p.1.

[11] M. Busio, O Steigelmann, Glastech. Ber. Glass Sci. Technol. 73 (2000) 319.

[12] J.D. Lee, Concise Inorganic Chemistry, Blackwell Scientific, Oxford, 1996.

[13] A. Van Die, A. C. H. I. Leenaers, G. Blasse,W.F. Van Der Weg, J. Non-Cryst. Solids 99 (1988) 32.

[14] A. V. Ziel, Solid State Physical Electronics, Prentice-Hall of India, New Delhi, 1971.

[15] A. Margaryan, A. Margaryan, J. H. Choi, F. G. Shi, Appl. Phys. B 78 (2004) 409.

[16] A. P. Vanýsek, Electrochemical Series, CRC Hand Book of Chemistry and Physics, Edited by D. R. Lide, CRC Press, London,1994, p. 22.

[17] A. Abragam and B. Bleaney, Electron Paramagnetic Resonance of Transition Ions, Oxford, Clarendon, 1970.

[18] D. Toloman, L. M. Giurgiu, I. Ardelean, Physica B (2009), doi:10.1016/j.physb.2009.07.187 (in press).

[19] J. W. H. Shreurs, J. Chem. Phys. 69 (1978) 2151.

[20] I. Ardelean, M. Peteanu, Gh. Ilonca, phys. status solidi A 58 (1986) 433.

[21] D. L. Griscom, R. E. Griscom, J. Chem. Phys. 47 (1967) 2711.

[22] P. C. Taylor, P. J. Bray, J. Phys. Chem. Solids 33 (1972) 43.

[23] I. Ardelean, Gh. Ilonca, M. Peteanu, Solid State Commun. 52 (1984) 147.

[24] I. Ardelean, M. Flora, J. Mater. Sci.: Mater. in Electronics 13 (2002) 357.

[25] J. S. Van Wieringen, Discuss. Faraday Soc. 19 (1955) 118.

[26] F. D. Tsay and L. Helmholz, J. Chem. Phys. 50 (1969) 2642.

[27] J. R. Pilbrow, Bull.Magn. Reson. 9 (1987) 32.

[28] B. T. Allen, J. Chem. Phys., 43 (1965) 3820.

[29] R. Dayal, D. Ramachandra Rao and P. Venkateswarlu, Can. J. Phys. 56 (1978) 1175.

[30] H. Togashi, N. Kojima, T. Ban, I. Tsujikawa, Bull. Chem. Soc. Jpn. 61 (1988) 1903.

[31] O. Sanz, E. Haro-Poniatowski, J. Gonzalo, J. M. Fernández Navarro. J. Non-Cryst. Solids 352 (2006) 761.

[32] Y. Zhang, Y. Yang, J. Zheng, W. Hua, G. Chen, J. Am. Ceram. Soc. 91 (2008) 3410.

[33] S. Zhou, N. Jiang, B. Zhu, H. Yang, S. Ye, G. Laksminarayana, J. Hao, J. Qiu, Adv. Funct. Mater. 18 (2008) 1407.

[34] M. A. Hamstra, H. F. Folkerts, G. Blasse, J. Mater. Chem. 4 (1994) 1349.

[35] X. G. Meng, J. R.. Qiu, M. Y. Peng, D. P. Chen, Q. Z. Zhao, X. W. Jiang, C. S. Zhu, Opt. Express 13 (2005) 1635.

Figure Captions

Fig. 1. TEM and SAED images of (a) 0 (base glass) and (b) 0.0058 atom % of MnO_2 doped glasses.

Fig. 2. EPR spectra of Mn^{2+} ions in (a) 0.0012, (b) 0.003 and (c) 0.0058 atom % of MnO_2 doped glasses.

Fig. 3. Optical absorbance spectra of (a) 0 (base glass), (b) 0.0012, (c) 0.003 and (d) 0.0058 atom % of MnO_2 doped glasses.

Fig. 4. Photoluminescence spectra of (a) 0 (base glass), (b) 0.0012, (c) 0.003 and (d) 0.0058 atom % of MnO_2 doped glasses excited at 400 nm.

Fig. 5. Photoluminescence spectra of (a) 0 (base glass), (b) 0.0012, (c) 0.003 and (d) 0.0058 atom % of MnO_2 doped glasses excited at 530 nm.

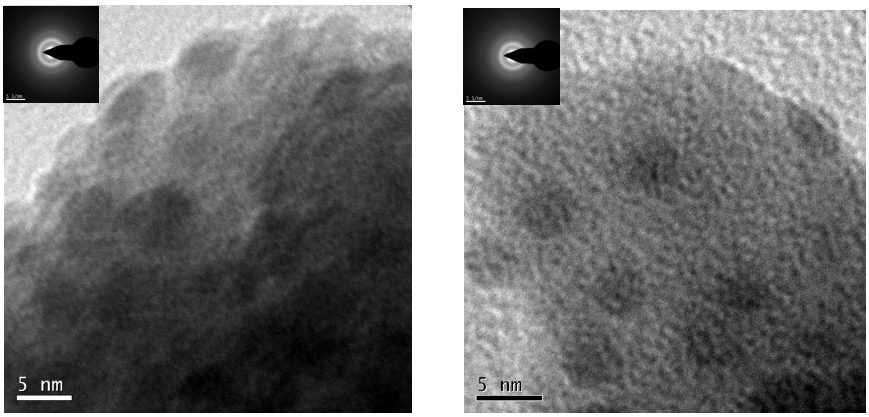

Fig. 1. TEM and SAED images of (a) 0 (base glass) and (b) 0.0058 atom % of MnO_2 doped glasses.

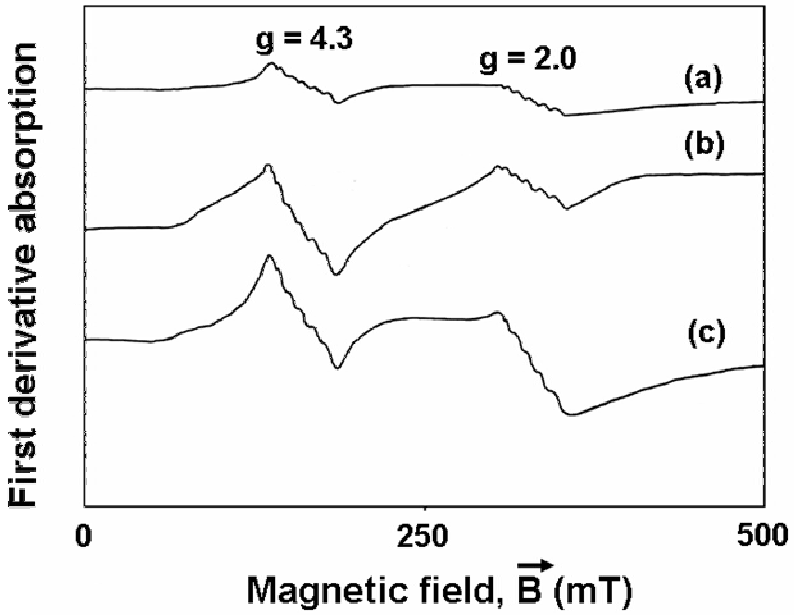

Fig. 2. EPR spectra of Mn^{2+} ions in (a) 0.0012, (b) 0.003 and (c) 0.0058 atom % of MnO_2 doped glasses.

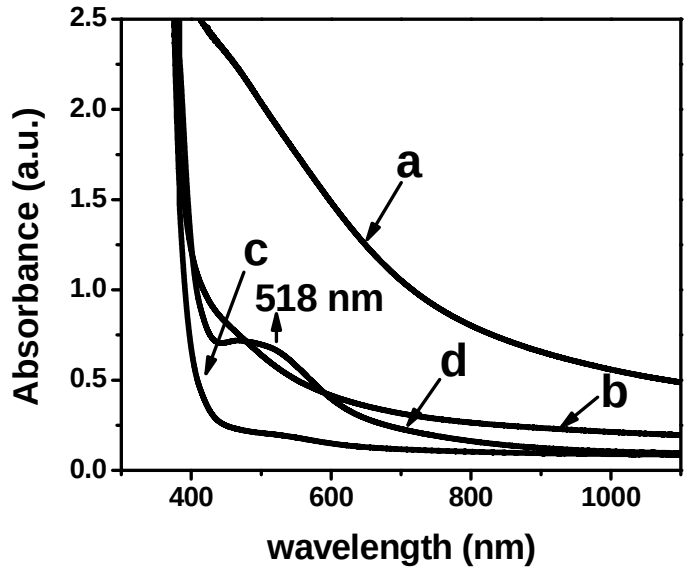

Fig. 3. Optical absorbance spectra of (a) 0 (base glass), (b) 0.0012, (c) 0.003 and (d) 0.0058 atom % of MnO_2 doped glasses.

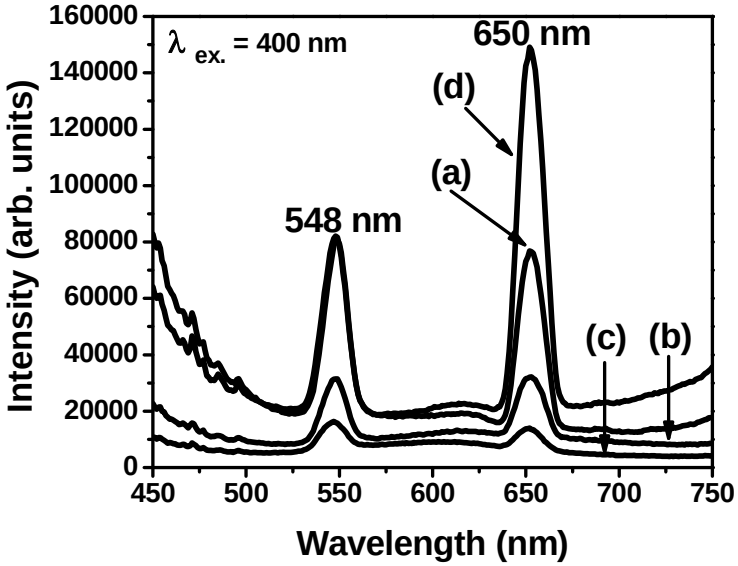

Fig. 4. Photoluminescence spectra of (a) 0 (base glass), (b) 0.0012, (c) 0.003 and (d) 0.0058 atom % of MnO_2 doped glasses excited at 400 nm.

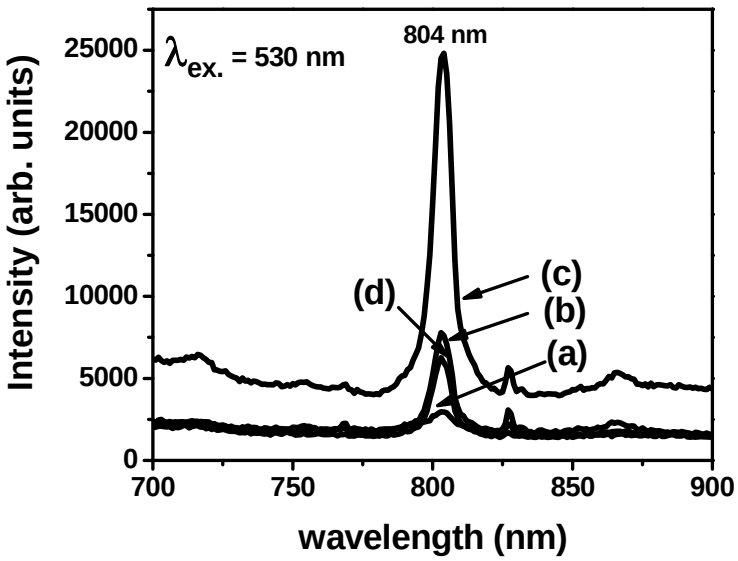

Fig. 5. Photoluminescence spectra of (a) 0 (base glass), (b) 0.0012, (c) 0.003 and (d) 0.0058 atom % of MnO_2 doped glasses excited at 530 nm.